Numerical Modelling and Simulation of a Lab-on-a-Chip for Blood Cells' Optical Analysis

Ahmed Fadlelmoula[1,2], Vítor Carvalho[3,4], Susana O. Catarino[1,2] and Graça Minas[1,2]
[1]*Center for MicroElectromechanical Systems (CMEMS-UMinho), University of Minho, 4800-058 Guimaraes, Portugal*
[2]*LABBELS–Associate Laboratory, Braga/Guimaraes, Portugal*
[3]*2Ai, School of Technology, IPCA, 4750-810 Barcelos, Portugal*
[4]*Algoritmi Research Center, University of Minho, 4800-058 Guimaraes, Portugal*

Keywords: Lab-on-a-Chip, Microfluidics, Numerical Simulation, COMSOL Multiphysics.

Abstract: Blood is a treasure of information about the functioning of the whole body. Thus, there is a continuous need for new, accurate, fast, and precise techniques to analyse blood samples. The goal of this work is to design and numerically simulate a low-cost lab-on-a-chip device, which, in the future, can be used to quickly diagnose diseases by using a tiny drop of a blood sample from the patient. The designed microdevice includes two fluid inlets, a serpentine area for achieving a continuous and fully developed flow, as well as a detection chamber able for optical measurements. The numerical model of the designed microdevice was computed using COMSOL Multiphysics software, taking into account the flow and tracking of microparticles, mimicking blood cells. In order to reach the best lab-on-a-chip geometry, i.e., achieving a high and stable number of particles in the detection chamber during the entire microfluidic assay, the inlet velocity, the channel width, and the diameter of the detection chamber were individually optimized. A mesh study was also performed to achieve the best results' accuracy, with lowest computational effort. From the achieved results, it was observed that a lab-on-a-chip geometry with a 0.5 mm channel width and a 2- or 3-mm detection chamber radius, with a fluid inlet velocity of 3 mm/s, was the one with the most interesting results for the intended application, with a constant number of particles flowing through the detection chamber (142 in average, for the selected inlet conditions).

1 INTRODUCTION

Blood is a treasure of information about the functioning of the whole body. Every minute, the entire blood volume circulates throughout the body, delivering oxygen and nutrients to every cell and transporting products from and toward all different tissues. As a result, blood harbors a massive amount of information about the functioning of all tissues and organs in the body Kouzehkanan et al., 2022). Consequently, blood sampling and analysis are of prime interest for medical and science applications and hold a central role in diagnosing several physiologic and pathologic conditions, localized or systemic. However, for clinical and scientific applications, it is necessary to understand, not only the biology, but also the technologies involved (Balogh, 2016). The knowledge about blood has always evolved in parallel with the general knowledge of biology, and several breakthroughs were facilitated by technological advances. More specifically, numerous devices are used to analyze blood cells with good sensitivity. Various techniques have been used for detecting platelets, white and red blood cells (Rohde, 2015), with a continuous need for fast, and precise techniques for the blood samples analysis. Microfluidics has demonstrated an enormous potential in this field. However, designing a customized microfluidic platform, and gaining a better understanding of its operation and the underlying physics and mechanics still pose significant technical challenges. On one hand, experimental approaches, although expensive and laborious, have been commonly used for the development of microfluidic devices since they are accurate and evidence-based methods (Fadlelmoula, 2022). Numerical approaches, on the other hand, are now recognized as a reliable complementary method aiming a reduction of cost, time, and effort, while being relatively accurate (Nagarajan, 2017). So, this

Fadlelmoula, A., Carvalho, V., Catarino, S. and Minas, G.
Numerical Modelling and Simulation of a Lab-on-a-Chip for Blood Cells' Optical Analysis.
DOI: 10.5220/0012571900003657

In *Proceedings of the 17th International Joint Conference on Biomedical Engineering Systems and Technologies (BIOSTEC 2024) - Volume 1*, pages 185-190
ISBN: 978-989-758-688-0; ISSN: 2184-4305

work aims to design, simulate and optimize a low-cost lab-on-a-chip (LOC) device, which can be used to quickly evaluate and analyze blood cells using optical methods. It presents the numerical modelling and the simulation study of an optimized microchannel geometry for the intended application. Therefore, it simulates the flow of a buffer fluid (representing plasma) filled with microparticles, mimicking flowing blood cells. The microdevice will comprise a serpentine region, for achieving a fully developed flow (Catarino, 2019), as well as a detection chamber, where the optical measurements will occur, where the number of particles/cells should be as high and steady as possible during the entire duration of the assays.

This paper is organized into 5 sections: Section 2 presents the numerical methods; Section 3 shows the obtained results; Section 4 presents the discussion; and Section 5 enunciates the conclusions and further developments.

2 NUMERICAL METHODS

This section describes the numerical simulation methods applied for simulating the designed microdevice.

2.1 2D Geometry Model

Figure 1 shows the initial lab-on-a-chip design geometry. According to the computational results (section 3), it will be optimized.

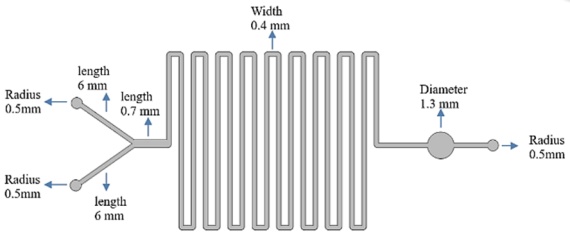

Figure 1: LOC initial design.

As can be observed in Figure 1, the total chip dimension, 2D top view, is 4 cm length and 1.6 cm width, there are 2 inlets and an outlet with a 0.5 mm radius. The serpentine turn width is 0.4 mm, and the circular detection chamber has a 1.3 mm diameter. Relatively to the domains' materials and properties, the microchannel walls are constituted by polydimethylsiloxane (PDMS) while, in the interior of the device, water (1000 kg/m³ density and 0.001 Pa·s viscosity) will be flowing (Norouzi, 2017).

2.2 Governing Equations

The COMSOL Multiphysics Laminar Flow interface (COMSOL, 2017) is used to compute the velocity and pressure fields for the flow of a single-phase fluid in the laminar flow regime. Equations (1) and (2) present the fluid flow governing equations:

$$\rho\left(\frac{\delta u}{\delta t} + u * \nabla u\right) = -\nabla P + \nabla.\tau \quad (1)$$

$$\tau = \eta\left(\nabla u + (\nabla u)^T\right) = 2\eta\, D \quad (2)$$

Where ρ represents the density, ∇ represents the gradient operator, u is the velocity vector, t is time, P is pressure, τ represents the Newtonian extra stress tensor, η is the dynamic viscosity, T is the matrix transpose, and D is the Symmetric rate of strain tensor.

Besides the laminar flow, particle tracing for the fluid flow was used as a numerical method for computing the paths and migration of individual particles by solving their equations of motion over time. The particle traceability will be examined under different conditions, to reach the maximum number of particles that will pass through the detection chamber. Equation (3) presents the particle tracing governing equation:

$$Ft = d(mpv)/dt \quad (3)$$

where Ft, mp, and v are, respectively, the total force, the particle mass, and the particle velocity. Particles moving through a fluid are subjected to a force, known as drag force, which acts in the direction of the fluid's motion relative to the object. Equation (4) presents the Stokes' law equation, that allows to determine the drag force (FD).

$$FD = 6\pi * \mu * rp * us \quad (4)$$

where rp is the radius of the sphere and us is the velocity of the fluid relative to the sphere, also called slip velocity.

2.3 Boundary and Initial Conditions

The following boundary and initial conditions were considered:

Laminar Flow: The default boundary condition in laminar flow is a non-slip wall, which means that the fluid velocity at the wall is zero.

Two different inlets were considered in the microchannel, one for the particle's inlet and other for the buffer solution (Inlet 1 and Inlet 2). Both of them are independently described by fluid velocities, that range from 1 to 8 mm/s. At the outlet, a zero pressure

boundary is set to assure the outflow. Regarding the numerical initial conditions, both initial velocity and pressure were set to zero.

Particle Tracing for Fluid Flow: The boundary condition in particle tracing was assumed as a slipping particle wall, which means particles reflect from the wall, such that the particle momentum is conserved.

Regarding the inlet of particles, these were released on both inlets, since the beginning of the assay (time = 0 s), and at time steps of 0.1 seconds, for a total duration of 15 seconds. At each 0.1 second release, 200 rigid, non-charged particles (as an approximation to flowing cells), entered the microchannel. The number of particles was selected, aiming to represent the number of blood cells in a diluted whole blood sample, flowing in the channel. In these simulations, the particles have a 5 μm diameter and a 1050 kg/m³ density, representing the size and density of red blood cells.

2.4 Mesh

After defining the numerical model, the geometry was meshed, aiming its computational solution. To reach the best type of mesh, aiming the most accurate results with lowest computational cost, a mesh study was performed. For that, simulations of the fluid flow were performed in three different regions of the microdevice, and the maximum fluid velocity was evaluated in each of those regions, as shown in Figure 2.

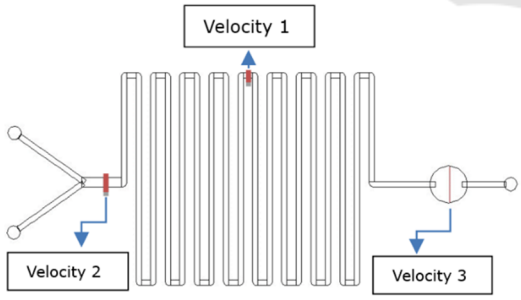

Figure 2: Schematic of the three regions where the maximum velocity was evaluated during the mesh study simulations.

After computing the model for 9 different meshes (predefined at COMSOL Multiphysics), the maximum velocity was evaluated in each of the 3 sections. Figure 3 shows the maximum velocity, at each of the three regions (Velocity 1, Velocity 2 and Velocity 3), for all the simulated meshes.

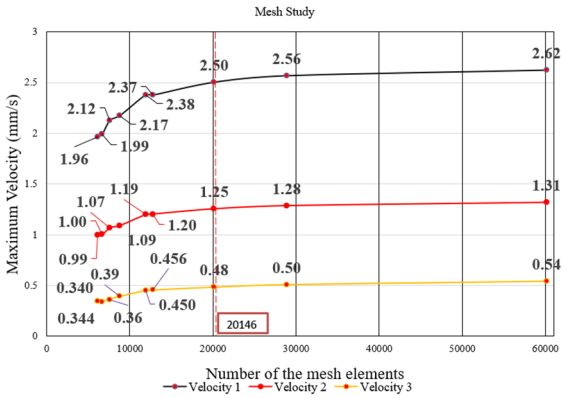

Figure 3: Maximum velocity (mm/s) in the microchannel as a function of the number of mesh elements.

From the presented plot, it can be observed that, above the 20146 elements mesh ("Finer" mesh, in COMSOL), even if the number of elements is increased (obviously with higher computational efforts, since the number of calculus points' increases significantly), there is no significant variation or improvement in the maximum velocity in any of the considered regions. As it reaches a plateau, it will be considered as the ideal mesh for this model, as it allowed to achieve accurate results, without an excessive computational cost (both regarding time and memory). Thus, the statistics of the selected "Finer" mesh, as predefined in COMSOL Multiphysics, are shown in table 1.

Table 1: Mesh Statistics.

	Minimum Element Quality	Average Element Quality	Mesh Vertices	Triangles
Finer	0.5016	0.8256	9351	20146

This mesh, with 20146 triangular elements (9351 of them mesh vertices), achieved the best results in terms of velocity stability and computational time. This mesh has a minimum element quality of 0.5016 (0-1 scale) and an average element quality of 0.8256, and it is represented in figure 4.

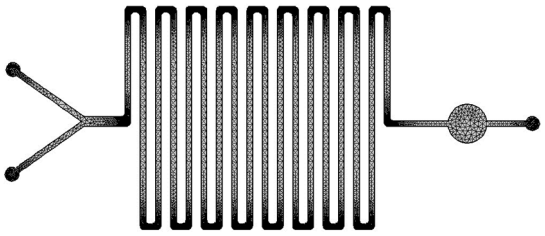

Figure 4: Representation of the 2D finer mesh.

2.5 Solver

The laminar flow, as a steady-state condition, was simulated using a stationary solver. The particle tracing was simulated considering a time-dependent solver, for a total duration of 15 seconds, with 0.1 s time steps.

3 RESULTS AND DISCUSSION

The simulated results, using COMSOL Multiphysics, were achieved considering the effect of the fluid flow (velocity and pressure profile along the lab-on-a-chip) and of the particle's migration in the detection chamber. For achieving a high and stable number of particles in the detection chamber during the entire microfluidic assay, the inlet velocity, the channel width, and the diameter of the detection chamber were individually optimized, outputting the best LOC geometry.

With the layout geometry described in Figure 1, Figure 5 shows the plot of the fluids' velocity magnitude during the migration along the microdevice. Analyzing Figure 6, that represents the velocity profile through a half-width cut of one of the simulated detection chambers, it can be concluded that the velocity in the near wall region decreases, being 0 at the wall, and being maximum at the center of the detection chamber. Moreover, figure 7 shows that the obtained pressure varies along the LOC channels from the highest at the beginning of the microdevice, decreasing gradually until the end of the microdevice.

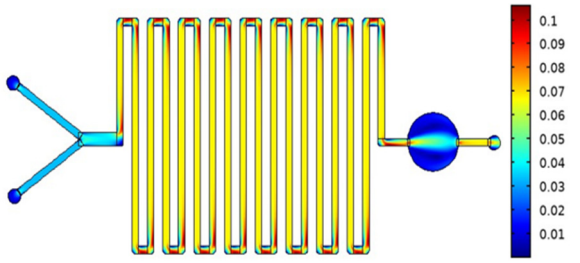

Figure 5: Stationary velocity magnitude (mm/s) in the microdevice.

The first layout geometry optimization was performed fixing the channel width and the detection chamber radius, and changing the inlet velocity. The channels' width was kept at 0.4 mm and the detection chamber radius as 1 mm. The velocity was changed being 1, 2, 3, 5 and 8 mm/s. Figures 8 show the average of the number of particles that passed through

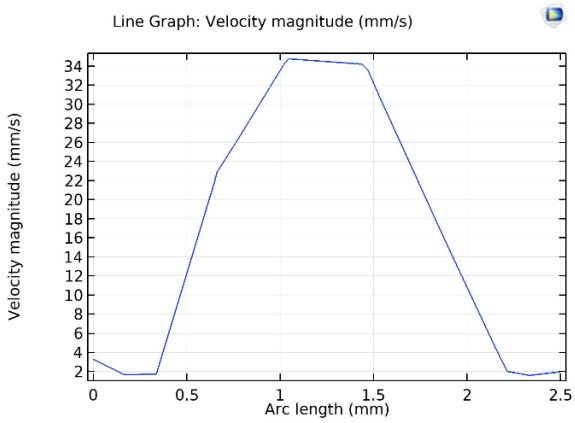

Figure 6: Example of a cross-section plot of the stationary velocity magnitude (mm/s), at the detection chamber half-width.

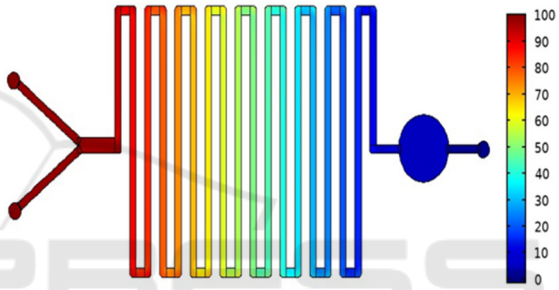

Figure 7: Pressure distribution along the microdevice.

the detection chamber, respectively, during the entire duration of the experiment (15 seconds). The results show that modifying the inlet velocity, from 1 to 8 mm/s, has no significant effect in the number of particles crossing the detection chamber (it was always around 25 particles at any time). As the 2 mm/s and 3 mm/s inlet velocities reached the exact same average results, a 3 mm/s inlet velocity was selected for the next optimization steps due to their slightly higher particles number passing through the detection chamber.

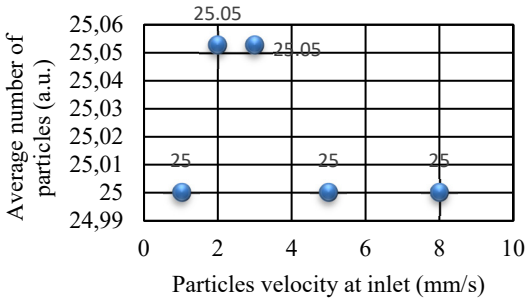

Figure 8: Average number of particles that passed through the detection chamber, for different inlet velocities.

In the second experiment, the channel width (0.4 mm) and the inlet velocity (3 mm/s) were fixed, and the detection chamber radius was changed from 1 to 3 mm in steps of 0.5 mm. Figures 9 and 10 show the average and standard deviation of the number of particles that passed through the detection chamber, respectively, during the duration of the simulation (15 seconds). The results show that, increasing the radius of the detection chamber leads to an increase of the average number of particles in that area. Thus, a 3 mm radius (with an average number of particles around 35) was selected for the next optimization steps.

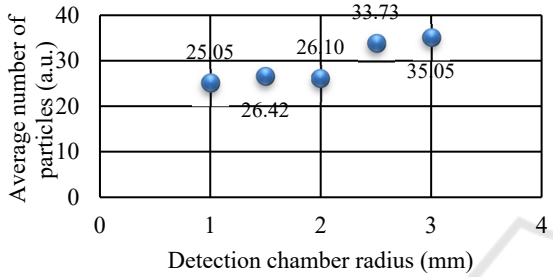

Figure 9: Average number of particles that passed through the detection chamber, for different detection chamber radius.

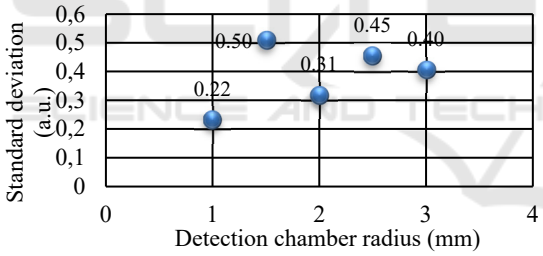

Figure 10: Standard deviation of the number of particles passing through the detection chamber, for different detection chamber radius.

In the third experiment, the inlet velocity (3 mm/s) and the detection chamber radius (3 mm) were fixed and the width of the channels was varied from 0.2 to 1 mm in steps of 0.1 mm. Figures 11 and 12 show the average and standard deviation of the number of particles that passed through the detection chamber during the duration of the assay (15 seconds), respectively. From the average and the standard deviation obtained results, an adequate channel width, combining a high and stable number of particles in the chamber is 0.5 mm.

Figure 13 shows the number of particles that passed through the detection chamber when changing the inlet 2 velocity and maintaining the previously optimized detection chamber radius (3 mm), channel width

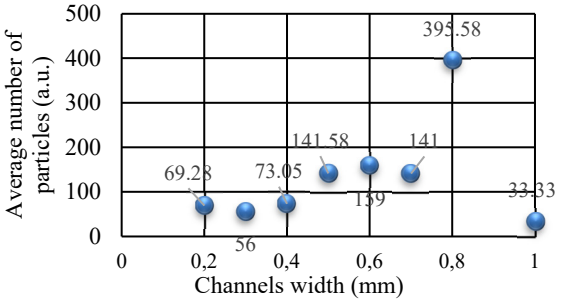

Figure 11: Average number of particles that passed the detection chamber, for different channels' width.

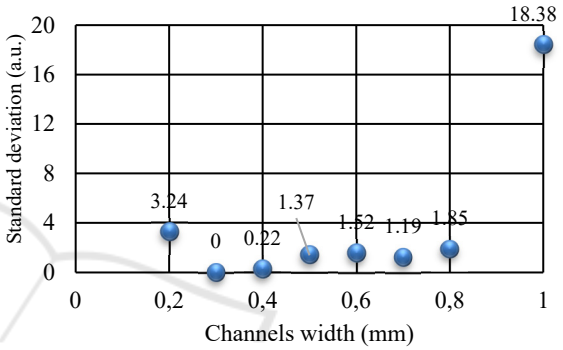

Figure 12: Standard deviation of the number of particles passing through the detection chamber, for different detection channels width.

(0.5mm) and inlet 1 velocity (3 mm/s). It was verified that no significant changes occurred regarding the particle number that passed in the detection chamber. This means that, for the studied geometries and inlet conditions, the change in the inlet 2 velocity (buffer) will not change the particle number.

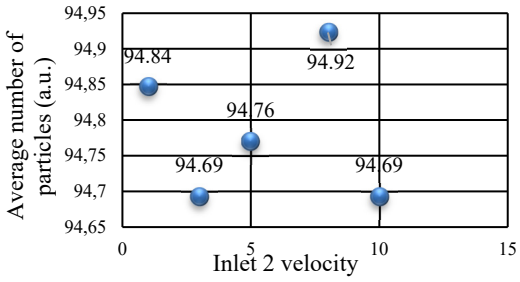

Figure 13: Average number of particles that passed the detection chamber, for different inlet 2 velocities.

From the results presented in the previous plots, Figure 14 shows the instantaneous number of particles passing through the detection chamber when a 0.5 mm channel width, a detection chamber radius

of 3 mm and an inlet velocity of 3 mm/s was considered. It can be observed that, after the particles first reach the detection chamber (shortly before 6 seconds), the number of particles keeps stable and almost constant during the assays.

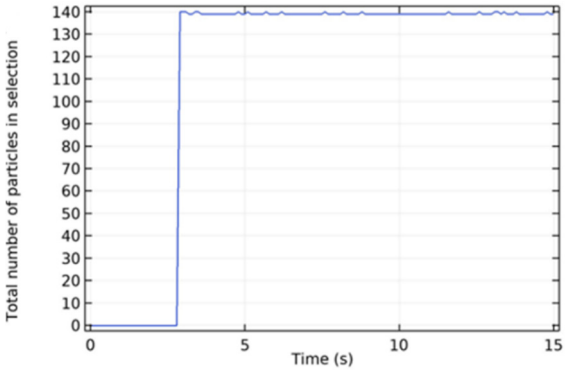

Figure 14: Total number of particles passing in the detection chamber over each time instant, considering the optimized design.

4 CONCLUSION AND FUTURE WORK

This works presented the design and numerically simulation of a LOC device with optimized dimensions, regarding inlets velocities, channel width, and diameter of the detection chamber for achieving a high and stable number of particles in the detection chamber. The numerical model was computed, using COMSOL Multiphysics software, taking into account the flow and microparticles tracking, mimicking the blood cells.

The obtained results showed the ideal design, a 0.5 mm channel width, a detection chamber radius of 2 mm or 3 mm, and an inlet velocity of 3 mm/s, achieving a total number of 142 particles flowing in the detection chamber (see figure 11). The change of the channels width made the major difference, when compared with the others changed parameters, in the number of particles passing through the detection chamber. Regarding the flow, the pressure along the LOC reached the maximum value at the inlet and decreased gradually until reached the minimum in the outlet. The stationary velocity reached the maximum value in the serpentine channels and at the center of the detection chamber.

Further work will consolidate the physical implementation of the simulated LOC model and their testing, examining the velocity, pressure, and particle flow inside the chip, and performing design updates if required.

ACKNOWLEDGMENTS

This work was supported by the R&D Unit Project Scope: UIDB/04436/2020, UIDB/05549/2020 and UIDP/05549/2020 funded by the Foundation for Science and Technology, I.P. (FCT). A.F. thanks the FCT for his 2023.03312.BD PhD grant. S.O.C. thanks the FCT for her 2020. 00215.CEECIND contract funding (DOI: 10.54499/2020.00215.CEECIND/CP1600/CT0009).

REFERENCES

Balogh, E. P., Miller, B. T., & Ball, J. R. (2016). Improving diagnosis in health care. In Improving Diagnosis in Health Care. National Academies Press. https://doi.org/10.17226/21794

Catarino, S. O., Rodrigues, R. O., Pinho, D., Miranda, J. M., Minas, G., & Lima, R. (2019). Blood cells separation and sorting techniques of passive microfluidic devices: From fabrication to applications. In Micromachines (Vol. 10, Issue 9). MDPI AG. https://doi.org/10.3390/mi10090593

COMSOL Multiphysics User's Guide. 2017. Available online: doc.comsol.com/5.4/doc/com.comsol.help.comsol/COMSOL_ReferenceManual.pdf (accessed on 1 September 2023).

Fadlelmoula, A., Pinho, D., Carvalho, V. H., Catarino, S. O., & Minas, G. (2022). Fourier Transform Infrared (FTIR) Spectroscopy to Analyse Human Blood over the Last 20 Years: A Review towards Lab-on-a-Chip Devices. In Micromachines (Vol. 13, Issue 2). MDPI. https://doi.org/10.3390/mi13020187.

Kouzehkanan, Z. M., Saghari, S., Tavakoli, S., Rostami, P., Abaszadeh, M., Mirzadeh, F., Satlsar, E. S., Gheidishahran, M., Gorgi, F., Mohammadi, S., & Hosseini, R. (2022). A large dataset of white blood cells containing cell locations and types, along with segmented nuclei and cytoplasm. Scientific Reports, 12(1). https://doi.org/10.1038/s41598-021-04426-x

Nagarajan, S., Stella, L., Lawton, L. A., Irvine, J. T. S., & Robertson, P. K. J. (2017). Mixing regime simulation and cellulose particle tracing in a stacked frame photocatalytic reactor. Chemical Engineering Journal, 313, 301–308. https://doi.org/10.1016/j.cej.2016.12. 016.

Norouzi, N., Bhakta, H. C., & Grover, W. H. (2017). Sorting (Multiphysics®)cells by their density. PLoS ONE, 12(7). https://doi.org/10.1371/journal.pone.0180520

Rohde, T., & Martinez, R. (2015). Equipment and Energy Usage in a Large Teaching Hospital in Norway. In Journal of Healthcare Engineering · (Vol. 6, Issue 3).